

“SMOOTH TRANSITION STRATEGY FOR DIFFERENT MODES OF OPERATION IN MICROGRID

¹Tatheer Banu, ²Dr.A.Srujana

¹M.Tech Student, ²Professor and Head of the Department

Department Of Electrical & Electronics Engineering

Vidya Jyothi Institute Of Technology, Hyderabad

ABSTRACT:- The ability of microgrids to operate in both grid-tied and island modes makes them special. Grid-forming or grid-following control techniques may be used by distributed energy resources (DERs) to function in any mode. While at least one DER in island mode must use a grid-forming approach, the majority of DERs in grid-connected mode utilise a grid-following control mechanism. As a result of an unplanned islanding event, the microgrid may experience significant variations in voltage and current. The two control strategies proposed in this work—a modified droop control that mimics the inertial behaviour of a synchronous generator and a linear voltage regulator with output current feedforward as input to the current regulator—help to achieve a smooth transition to island mode and lessen the interference effect. The recommended controller facilitates a seamless transition and minimises changes in voltage, current, and frequency. Small-signal analysis is used to determine the coefficients of the proposed control mechanism and the destabilising

effects of continuous power demand (CPL). The results of the trials support the efficacy of the recommended control strategy.

“Index Terms—Grid-connected, islanding mode, microgrids, modified droop control, smooth transition”.

1. INTRODUCTION

A microgrid may run in both grid-tied and island mode (IS) since it is a tiny power system (GC). Several methods may be used to manage distributed energy resources (DER) in microgrids, depending on the operating mode (MGs). DERs are often the most crucial component of MG, and they are built on power electronic converters. The use of grid-forming control methods or grid-following control strategies may make DERs work as voltage sources or current sources, respectively [1].

The former is beneficial for converters that only pump a certain current into the MG, as those used in renewable energy sources, while the latter may

be utilised in any operating mode (RES). Since the upstream grid regulates the voltage and frequency of the MG in GC mode, DERs often operate in tandem with it. But in island mode, a certain set of DERs must be used in a grid-forming approach in order to regulate the voltage and frequency of the MG. The stability and hardness of MG are impacted by DERs. The research has presented a number of DER control mechanisms that may be used to both GC and IS operating modes. These restraint methods may be divided into two groups. One of two options involves control techniques with two distinct control schemes, where each operating mode is applied in accordance with a predefined control target. Control methods with a single control scheme that is further provided for both operating modes are the alternative (usually based on voltage control). capabilities. Nonlinear control theory served as the foundation for many of the early controller types, including Lyapunov-based techniques and model predictive control. These techniques often made use of a dynamic DER behaviour and an ideal system model. These controllers are extremely difficult to install, however, owing to their intricate design and high computational costs. It might be difficult to put these control mechanisms into action. On the other hand, linear control systems have excellent design and implementation simplicity, a simple architecture, and minimal computational costs. The performance of the controller is best understood using linear control techniques, which use feedback or feedforward of physical variables. Cascaded control systems have been used to the design and implementation of controls in the past. These controllers must be capable of switching seamlessly between the two modes of operation. This

adjustment should be smooth or at the very least stay within acceptable parameters. During the changeover, the following might provide problems: 1) Frequency jitter caused by transitioning from the grating-following to the grating-forming mode, which jeopardises MG stability and messes with DER power angles; and 2) Mode switching-induced voltage and current changes at the DER output.

You may alternate between GC and IS mode or IS and GC mode in MGs. The first condition explains the synchronisation procedure where the grid connection's (PCC) voltage must be monitored. According to IEEE.std.1547-2003, the conventional limitations for synchronisation requirements are 10% voltage amplitude difference, 0.3 Hz frequency difference, and 20 degree phase difference. The appropriate synchronisation approach is adopted, which prevents the stoppage of MG and transfer hinges. The second scenario (i.e., switching from GC to IS mode) may happen purposefully or accidentally. Temporal intensity may be maintained with targeted island generation by altering the MG operating point. The fact that the functioning point of DERs cannot be modified, resulting in inadvertent islanding, is a key worry of this study. As a result, the frequency and voltage amplitude of the MG alter significantly, endangering the stability of the system. Several interventions have been documented in the literature to lessen the consequences of transition process abnormalities. When employing droop-based control mechanisms, there is no need to switch between the controls utilised in the two modes. Techniques for nonlinear control are an option. The authors outline a nonlinear control method that employs adaptive back-stepping in two

operating modes. Investigated is the potential for variable structure-based nonlinear control to reduce important disruptions like islanding. It is advised that single-phase inverters be operated in both modes using model predictive control. Autotuning weight variables and hybrid objective functions are used in this MPC system. The smooth transition between operating modes has mostly been researched for MGs with a single DER, even though in actuality MGs have many DERs with various buses. In this case, it is crucial to carefully examine how different DER controllers interact with one another. The power sharing between the DERs during the transition determines the usual power angle variation related with this interaction. The power angle and frequency are drastically changed while operating in discrete mode. The damping ratio needs to be raised for a smooth transition. Reduce frequency oscillations during MG conversion by using virtual inertia. Two other applications of virtual inertia are droop control and a virtual synchronous generator (VSG). The dynamic performance of the small-signal model of VSG control and droop control differs, despite certain similarities. The VSG droop was shown to occur more slowly than the control. Actual derate control, however, is more predictable than VSG output. When used with VSG control, a governor delay causes the oscillations to worsen. This method offers both VSG and transient mode inertial behaviour since droop control is often employed in microgrid applications. If the droop control parameters are correctly changed in accordance with the system requirements, the dynamics may be enhanced.

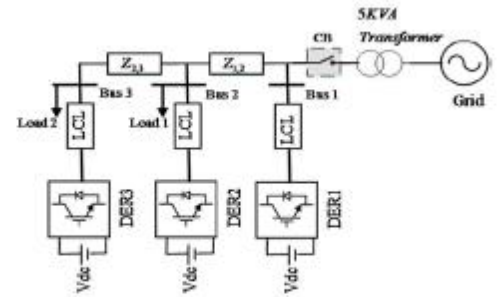


Fig. 1. Schematic of a MG including three converter-based DER.

VSGs are less potent than inverters. To account for virtual inertia, a modified droop control must be given even if a derivative term is added to the droop mechanism to enhance power distribution. In order to facilitate a smooth transition from GC to IS mode, optimum load sharing amongst DERs, and increased system stability, this research suggests a control technique that alters conventional droop control and voltage management. The main contributions of this work fall under the following categories of anomalies that deal with the tremendous complexity of nonlinear techniques or the unreliable performance of linear methods: 1) Output current bias raises voltage. A modified linear voltage control method is used to produce a capacitor current feedback provision coupled to the loop and high pass filter to each current loop. By enhancing damping, lessening the impacts of noise, and correcting for transient voltage drop at the inverter output, this strategy enhances the dynamic performance of the system. Engineers can utilise it with ease because of how easy it is. 2) A modification to the droop mechanism allows it to adjust its coefficient in response to variations in active power. In the case of faults, this process, which is brought on by the synchronous generator's inertial nature, results in undesired frequency overshoot or undershoot. To assess how well the

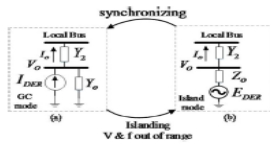


Fig. 4. DER equivalent circuit in both (a) grid-feeding control strategy and (b) grid-forming control strategy.

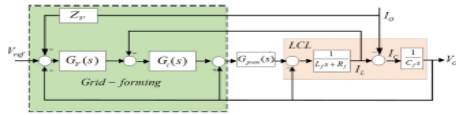


Fig. 5. Block diagram of conventional VCM with output voltage and inductor current feedback and virtual impedance.

derived as:

$$I_o = \underbrace{G_c(s)}_{IDER} I_{ref} - Y_o V_o \quad (2)$$

Norton displays the relevant circuit. As a consequence, the analogue circuit shown in Figure 4(a)[26] serves as the DER's representation in this mode. Draw the corresponding circuit layout for an admittance y_o and a constant current source linked in parallel. A line admittance known as Y_2 connects the converter's output to its local bus in this area.

2.2. Islanding Mode

Cascade loops [16, 17], which include power controllers, voltage controllers, and current controllers, are the foundation of a network-forming control mechanism. The power regulator acts as a simple droop controller by giving the internal loops voltage amplitude and phase references. A simple droop mechanism has the following expression:

$$\omega = \omega^* - m(P - P^*), E = E^* - n(Q - Q^*) \quad (3)$$

The letters E and E, respectively, stand for output voltage amplitude, inverter voltage amplitude, and reference angular frequency. P and Q indicate the measured active and reactive power output, respectively, after passing through a low-pass filter with a low cut-off frequency, where P and Q

represent the active and reactive power references (wc). M and n, the droop coefficients A example block diagram for a VCM may be seen in Figure 5. The basic VCM's closed loop transfer function is stated as (4).

$$V_o = \frac{G_v(s)G_i(s)G_{pwm}(s)}{L_f C_f s^2 + R_f C_f s + G_i(s)G_{pwm}(s)(G_v(s) + C_f s) + 1 - G_{pwm}(s)} V_{ref} - \frac{L_f s + R_f + G_i(s)G_{pwm}(s)(G_v(s)Z_v(s) + 1)}{L_f C_f s^2 + R_f C_f s + G_i(s)G_{pwm}(s)(G_v(s) + C_f s) + 1 - G_{pwm}(s)} I_o \quad (4)$$

“Where V_{ref} is the reference voltage and $G_v(s)$ is the voltage controller transfer function. the potential output voltage (4)”.

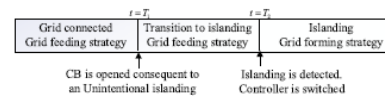


Fig. 6. The time procedure of an unintentional islanding.

described by $G_{conv}(s)$ is the closed-loop transfer function of the conventional VCM strategy.

$$V_o = \underbrace{G_{conv}(s)}_{EDER} V_{ref} - Z_o^{conv} I_o \quad (5)$$

$$\begin{cases} G_{conv}(s) = \frac{G_v(s)G_i(s)G_{pwm}(s)}{L_f C_f s^2 + R_f C_f s + G_i(s)G_{pwm}(s)(G_v(s) + C_f s) + 1 - G_{pwm}(s)} \\ Z_o^{conv}(s) = \frac{L_f s + R_f + G_i(s)G_{pwm}(s)(G_v(s)Z_v(s) + 1)}{L_f C_f s^2 + R_f C_f s + G_i(s)G_{pwm}(s)(G_v(s) + C_f s) + 1 - G_{pwm}(s)} \end{cases} \quad (6)$$

For a number of applications, including g, the output impedance Z_{conv} is changed by virtual impedance (Z_v). partition of power [27]. According to, DERs might be replicated via Thevenin equivalent circuits (5). A lattice building method-based analogue circuit for a DER is shown in Figure 4(b). It consists of an impedance Z_o and a voltage source connected in series.

2.3. Transition between Modes

Contrary to intentional islanding, the DER controller's setpoint or operating point cannot be modified right away in the event of an accident. The voltage and current output of the DER may

fluctuate dramatically because of the low inertia of the power electronic converters in this situation. The DER controller effect has a significant impact on the size and duration of the transition mode fluctuations. To maintain the system stable within a particular range and to survive large changes, an island controller is necessary. FIG. depicts the change from grid linked MG to island mode. MG is envisioned to run in grid-tied mode. Due to unintentional islanding, the circuit breaker trips at time $t = T1$. The island detection method allowed for simple verification of island presence. A mode transfer signal is issued at time $t=T2$ (switch to grating-forming technique). DERs continue to run in T1 to T2 grid feed mode as a consequence.

2.4. Proposed Control Strategy

This section's goal is to provide DERs a main level control mechanism so they can function well even when islanding causes them to mistakenly flip from GC to IS mode. In FIG., the suggested control method for a converter-based DER is architecturally shown. The control system in Figure 2 includes a smooth transient compensator to guarantee that fluctuations are maintained to a minimum. The compensator's two inputs are the output current and the capacitor current (I_c) (I_o). The necessary output signals are provided by two distinct transfer functions, which are then merged.

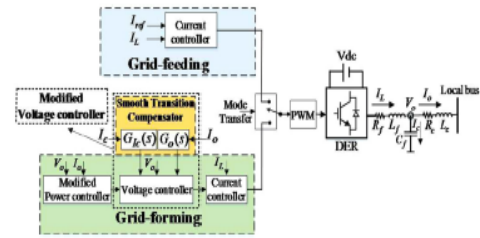


Fig. 7. Overall structure of the proposed control strategy for a converter-based DER.

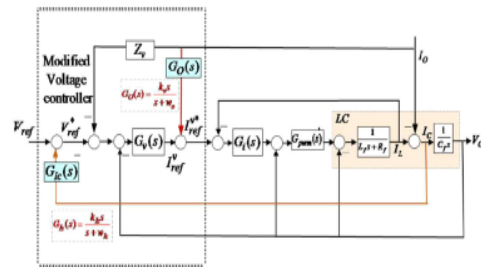


Fig. 8. Block diagram of the proposed control strategy with modified voltage controller in islanding mode.

voltage regulator It is said that a voltage regulator has been changed if it has a smooth transient compensator. an appropriate voltage regulator, 1. The efficacy of the regulator has an impact on the extent and duration of the deviations. The voltage regulator has to slow down even more so that the amplitude and length of the deviations remain within a reasonable range. The new voltage reference may be discovered by including capacitor current feedback in the voltage loop and looks like this:

$$V_{ref}^* = V_{ref} - G_{Ic}(s)I_c \tag{7}$$

“where $G_{Ic}(s)$ is a high pass filter and I_c is the capacitor current. The $G_{Ic}(s)$ symbol is”:

$$G_{Ic}(s) = \frac{K_{Ic}s}{s + w_{Ic}} \tag{8}$$

The cutoff frequency is w_{Ic} , and the gain is K_{Ic} . The VCM technique in FIG. 5 is converted to FIG. by this input. By combining (7) and (8), the closed

loop output voltage transfer function (V_o/V_{ref}) is created (5).

$$V_o = G_{conv}(s)V_{ref}^* = G_{conv}(s)(V_{ref} - G_{Ic}(s)I_c) \quad (9)$$

Using $I_c = C_{fs}V_o$ one can write:

$$V_o = G_{conv}(s)(V_{ref} - G_{Ic}(s)C_{fs}V_o) \quad (10)$$

The closed loop transfer function's final form is as follows:

$$V_o = \frac{G_{conv}(s)}{1 + G_{conv}(s)G_{Ic}(s)C_{fs}} V_{ref} = G_{proposed}(s)V_{ref} \quad (11)$$

The suggested controller's efficacy is assessed using frequency analysis and step response in the time domain.

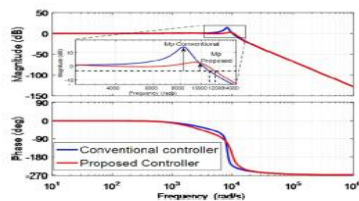


Fig. 9. Frequency response of the closed-loop transfer function (V_o/V_{ref}) of $G_{conv}(s)$ and $G_{proposed}(s)$ with $K_{Ic} = 15$ and $w_{Ic} = 400\text{Hz}$.

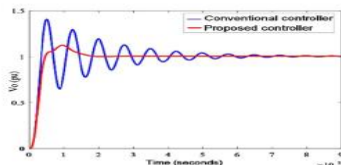


Fig. 10. Step response of the closed-loop transfer function (V_o/V_{ref}) of $G_{conv}(s)$ and $G_{proposed}(s)$ with $K_{Ic} = 15$ and $w_{Ic} = 400\text{Hz}$.

Response studies exist. The findings of the closed loop tracking voltage transfer functions $G_{proposed}(s)$ and G_{conv} in relation to the frequency response sensitivity are shown in Figure 9. (s). It is obvious that the suggested controller reduces the frequency response's maximum magnitude. The proposed controller, as can be seen, has a wider bandwidth than the existing controller. Figure 10 contrasts the efficacy of the suggested controller with G_{conv} by displaying their phase responses. The output current (I_o) is a disturbance

variable, as shown by the streamlined block diagram of the control strategy with LC filter system in Figure 5. The relationship between output voltage and output current is well acknowledged (5). As a result, variations in output current have a direct impact on output voltage.

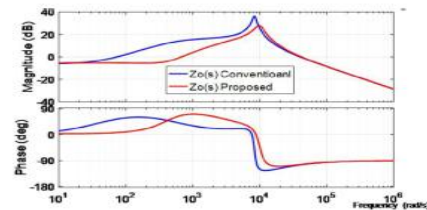


Fig. 11. Frequency response of the closed loop transfer function of (V_o/I_o) for conventional (Z_o^{conv}) and proposed controller ($Z_o^{proposed}$).

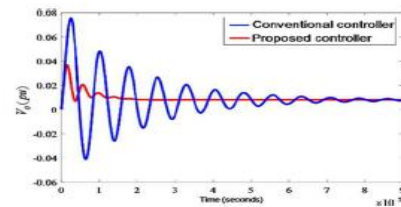


Fig. 12. Step response of the closed loop transfer function of (V_o/I_o) for conventional (Z_o^{conv}) and proposed controller ($Z_o^{proposed}$).

To lessen the impact of the output current disturbance on the output voltage, a feed forward of the output current is added to the voltage regulation method known as the input of a current regulator (see Fig. 8). As a consequence, the following is the new command for the present controller:

$$I_{ref}^{v*} = I_{ref}^v + G_o(s)I_o \quad (12)$$

To lessen the impact of output current variations on the output voltage, the output current feedforward is introduced to the proposed voltage control mechanism as the input of the current regulator (see Fig. 8). As a consequence, the following is the new command for the present controller:

$$G_o(s) = \frac{K_o s}{s + w_o} \quad (13)$$

The gain and cutoff frequency are referred to here as Z_o and V_o respectively. The feed-forward current is used to transform the closed-loop transfer function $(V_o \ I_o)$ in equation (6):

$$Z_o = Z_o^{conv} - G_i(s)G_{pwm}(s)G_o(s) \quad (14)$$

By taking into account the capacitor current feedback in Fig. 8, as shown below, it is feasible to determine the equivalent output impedance of the suggested control mechanism:

$$Z_o^{proposed} = \frac{L_f s + R_f + G_i(s)G_{pwm}(s)(1 + G_v(s)Z_v - G_o(s))}{L_f C_f s^2 + R_f C_f s + G_i(s)G_{pwm}(s)(G_v(s) + G_v(s)G_{lc}(s)C_f s + C_f s) + 1 - G_{pwm}(s)} \quad (15)$$

Figures 3 and 4, respectively, show the frequency and phase responses of the suggested and traditional output impedance approaches. The suggested approach is different from this since it has a larger bandwidth and a lower resonance frequency peak. As can be observed, the suggested method lowers the gain throughout a large spectrum of frequencies, leading to a considerable decrease in interference. The suggested approach also considerably lowers oscillation and overshoot (see Fig. 12). Last but not least, the boosted voltage regulator transfer function is:

$$\begin{cases} G_{proposed}(s) = \frac{G_v(s)G_i(s)G_{pwm}(s)}{\Delta} \\ Z_o^{proposed} = \frac{L_f s + R_f + G_i(s)G_{pwm}(s)(1 + G_v(s)Z_v - G_o(s))}{\Delta} \\ \Delta = L_f C_f s^2 + R_f C_f s + G_i(s)G_{pwm}(s) \\ \times (G_v(s) + G_v(s)G_{lc}(s)C_f s + C_f s) + 1 - G_{pwm}(s). \end{cases} \quad (16)$$

B. Modified Droop Control

As was previously established, there is a phase shift or jump in the output voltage when switching

between two regulators, increasing the deviations in the output voltage and current. The closed transfer function (16) of the inner loops (current regulator and voltage regulator) demonstrates unity gain and zero phase shift across a broad frequency range. Therefore, based on the droop mechanism, the power controller in this work can estimate the phase and amplitude of the DER output voltage. The output voltage reference created by droop control may be specified as [16]:

$$V_{ref} = E \sin(\omega^* t + \varphi) \quad (17)$$

E denotes the voltage amplitude, angular frequency, and phase references created by (5). Even though simple droop has numerous benefits, phase drift caused by mode or load changes on the island compromises MG stability. To fix this issue, the following methods may be used to a fundamental frequency droop mechanism:

$$P - P^* = \frac{1}{m}(\omega - \omega^*) + T_{wc} \frac{1}{m} s\omega \quad (18)$$

T_{wc} stands for the low-pass filter's time constant in droop control, T_{wc}/m for its equivalent moment of inertia, and T_{wc}/m and T_{wc}/m for its associated damping coefficients. By lowering m , the system's inertia increases, which results in less phase deviation. To correctly change its coefficient, a modified droop control is advised. The revised droop controls frequently include the following characteristics:

$$\omega = \omega^* - f_i \left(m, P, \frac{dP}{dt} \right) \quad (19)$$

“One can write the function $f_i(\cdot)$ of (19) as”.

$$f_i\left(m, P, \frac{dP}{dt}\right) = \underbrace{me^{-\beta\left|\frac{dP}{dt}\right|}P}_{\text{Proposed nonlinear term}} - \underbrace{m_d\frac{dP}{dt}}_{\text{Derivative term}}$$

“the Q – E droop equation is introduced as follows”:

$$E = E^* - nQ - n_d\frac{dQ}{dt} \tag{21}$$

where the letters md, nd, and, respectively, stand in for the derivative coefficients and the exponential coefficient. The efficiency and stability of the derivative term are examined in [8] and [16]. When dp/dt is equal to zero, the proposed droop control behaves as the usual droop (stationary state). A dead-band is used for dp/dt to avoid enabling against minor oscillations.

2.5. Small Signal Analysis

To guarantee MG stability, recommended control technique parameters must be set up. Figures 9–12 illustrate how inner loops function. Given that a power controller is a straightforward control circuit, it should be obvious that, when taken into account independently [16], [26], its dynamic behaviour may be disregarded. The revised droop controllers' stability was evaluated using a fast signal analysis. The following formula [16] is used to represent the power injection of a DER linked to the grid via reactance:

$$P = \frac{EV}{X} \sin \varphi \tag{22}$$

$$Q = \frac{EV}{X} \cos \varphi - \frac{V^2}{X} \tag{23}$$

“One may write: by linearizing (22) and (23) about a certain operation point”.

$$\begin{bmatrix} \Delta P \\ \Delta Q \end{bmatrix} = \frac{w_c}{s + w_c} \frac{V}{X} \begin{bmatrix} \sin \Phi & E \cos \Phi \\ \cos \Phi & -E \sin \Phi \end{bmatrix} \begin{bmatrix} \Delta E \\ \Delta \varphi \end{bmatrix} \tag{24}$$

The minor annoyances in this instance that surround the operative point are P, Q, E, and. The operating point variables are E and V, and the output reactance is X. The following steps are required to construct the linear model of the recommended droop control with e = (1 +):

$$\omega = \omega^* - m\left(1 - \beta\frac{dP}{dt}\right)P - m_d\frac{dP}{dt} \tag{25}$$

The previous equation is perturbed around the equilibrium point and the following assumptions are made to create the Laplace versions of (25) and (21):

$$\Delta\omega = \Delta\omega^* + (-m + \beta m P_0 s - m_d s)\Delta P \tag{26}$$

$$\Delta E = \Delta E^* - n\Delta Q - n_d s\Delta Q \tag{27}$$

When (24), (26), and (27) are used, the tiny signal model is:

$$s\Delta\varphi = \Delta\omega = (-m + \beta m P_0 s - m_d s) \times \frac{w_c}{w_c + s} \frac{V}{X} [\sin \Phi \Delta E + E \cos \Phi \Delta\varphi] \tag{28}$$

$$\Delta E = -(n + n_d s) \frac{w_c}{w_c + s} \frac{V}{X} [\cos \Phi \Delta E - E \sin \Phi \Delta\varphi] \tag{29}$$

By substituting (29) into (28), one can write

$$s\Delta\varphi = (-m + \beta m P_0 s - m_d s) \times \frac{w_c}{w_c + s} \frac{V}{X} \times \left[\frac{(n + n_d s) w_c \frac{V}{X} E \sin \Phi}{(w_c + s + w_c (n + n_d s) \frac{V}{X} \cos \Phi)} \Delta\varphi + E \cos \Phi \Delta\varphi \right] \tag{30}$$

“Finally, the characteristic equation is calculated as”:

$$s^3 + As^2 + Bs + C = 0 \tag{31}$$

$$A = \frac{w_c}{X_d} \left[2X + nV \cos \Phi + n_d w_c V \cos \Phi + m_d EV \left(w_c n_d \frac{V}{X} + \cos \Phi \right) + VE\beta m P_0 \left(w_c n_d \frac{V}{X} + \cos \Phi \right) \right] \tag{32}$$

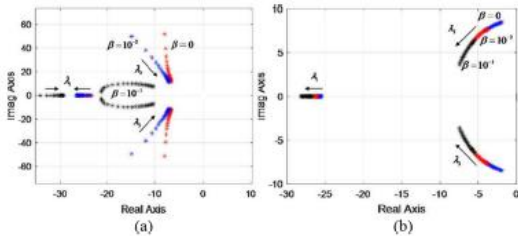


Fig. 13. Root loci of the system considering the proposed solution: (a) $\beta = 0, 10^{-2}$ and 10^{-1} and $m_d = 7 \times 10^{-7}$ for $10^{-6} \leq m \leq 32 \times 10^{-5}$, (b) $\beta = 0, 10^{-2}$ and 10^{-1} and $m = 32 \times 10^{-5}$ for $10^{-7} \leq m_d \leq 10^{-6}$.

$$B = \frac{w_c}{X_d} \left[Xw_c + nw_c \frac{V}{X} \cos \Phi + mEV \cos \Phi + mn_d w_c \frac{V}{X} \dots + m_d EVw_c \left(n \frac{V}{X} + \cos \Phi \right) + VE\beta m P_0 w_c \left(n \frac{V}{X} + \cos \Phi \right) \right] \tag{33}$$

$$C = w_c^2 \frac{V}{X_d} mE \left(n \frac{V}{X} + \cos \Phi \right) \tag{34}$$

Dr. Xd X+ndwcVcos, Using the characteristic equation and the variables mentioned in Table I, the root locus is shown in FIG. 13. Figure 13(a) depicts the origin of the system for various values of m. The origin of the system is m. It turns out that when the real component grows, the complex eigenvalues (2, 3) move closer to the real axis. More dumping will occur as a result. Figure 13 depicts where the system started for various md and (b). To enhance the system's dynamic performance, complex eigenvalues are utilised as parameters and increments with big real parts and tiny imaginary parts. This kind of dynamic stress should be acknowledged. B. engines that have an impact on the system's dynamics. This dynamic is known as the CPL in small-signal stability studies [28]. A basic small-signal model of MG with loads is shown in [29]. A very modest signal model of the test MG is built to assess how well the suggested controller performs under dynamic loads. The usual

MG small signal test model is described as follows:

XXX

$$\begin{bmatrix} \Delta x_{INV} \\ \Delta i_{lineDQ} \\ \Delta i_{loadDQ} \end{bmatrix} = A_{MG} \begin{bmatrix} \Delta x_{INV} \\ \Delta i_{lineDQ} \\ \Delta i_{loadDQ} \end{bmatrix} \tag{35}$$

The model matrices in [29] were created using the parameters in the table. I. The major values of the model are shown in Fig. 14. According to the usual method, the system contains eigenvalues with positive real portions, as shown in Fig. 14. (a). These favourable eigenvalues rise as CPL resistance falls. To decrease the destabilising effects of CPL, the suggested technique, shown in Fig. 14, may shift positive eigenvalues toward the left hemiplane (b).

3. FUZZY LOGIC

Fuzzy logic applications have grown dramatically in both quantity and diversity during the last several years. Applications for consumer gadgets including cameras, camcorders, washing machines, and microwaves as well as portfolio selection in the workplace and industrial process control are also mentioned.

You must first comprehend fuzzy logic in order to comprehend why it is so prevalent.

One of two things may be indicated by fuzzy logic. A constrained version of multivalve logic's logic framework is fuzzy logic. In a broad sense, fuzzy sets theory and fuzzy logic (FL) are basically related since they both deal with classes of objects that have fuzzy bounds and degree-dependent membership. This argument claims that, in the strictest sense, fuzzy logic is a subset of fl. Even in

its more constrained version, fuzzy logic differs logically and qualitatively from traditional multi-valve logic systems. It is best to think of the fuzzy logic used in the Fuzzy Logic Toolbox programme as FL, or fuzzy logic in its widest sense. Clear explanations of FL's fundamental ideas are given in Fuzzy Logic Basics, along with helpful examples. It should be highlighted that the fundamental concept of FL is a language variable, or a variable with word values as opposed to numeric values. The majority of FL might be seen as a computing method that relies on words rather than numbers. Words are naturally less accurate than numbers, yet their usage is consistent with human perception. Another benefit of word-based computing is the ability to tolerate mistakes and lower response costs.

4. SIMULATION RESULTS

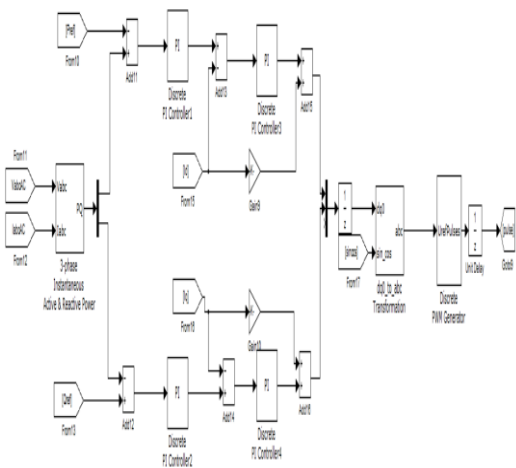


Fig . Code blocks for PI controller.

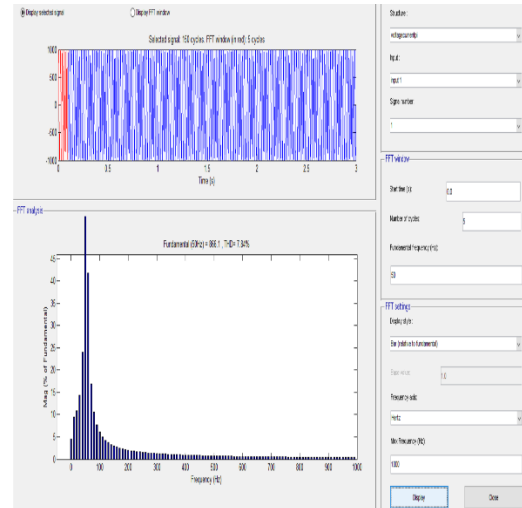


Fig. Harmonic distortion for PI controller.

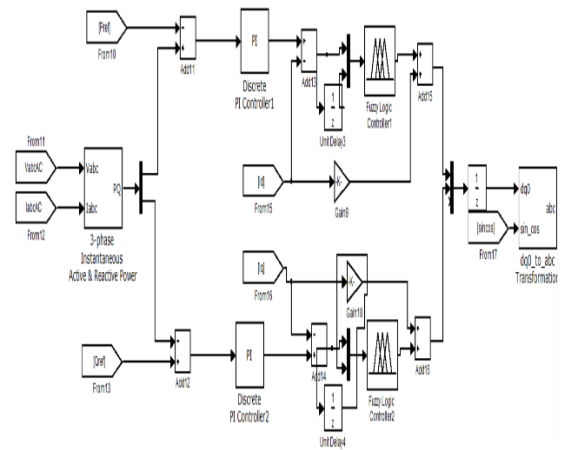


Fig . Code blocks for fuzzy logic controller.

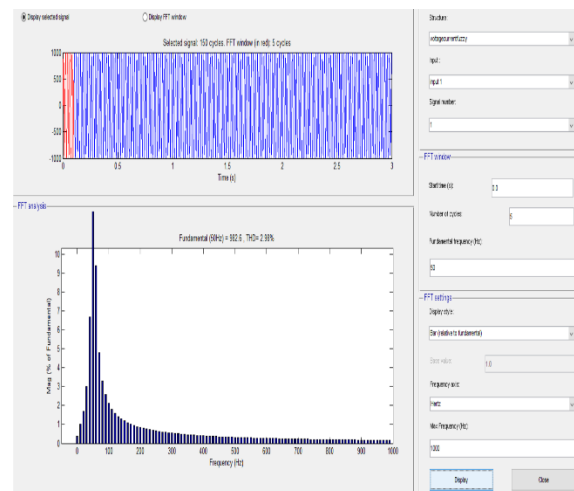


Fig . Harmonic distortion for fuzzy logic controller.

5. CONCLUSION

This study offers a helpful control technique for a seamless switch from grid to island mode caused by unintentional islanding. Two compensators—capacitor current feedback, output current feedforward loops, and a modified decay mechanism—make up the suggested control strategy. The frequency variance is brought down to a bearable level using the suggested droop control. Both the frequency and time domains are used to assess the compensator's performance. The effectiveness of the suggested controller in lowering overshoot, boosting bandwidth, and enhancing damping is shown by simulation results.

Small signal analysis was utilised to choose the best coefficients for improved droop control. A particular small-signal stability was tested at various CPL levels in order to gauge the destabilising impact of CPL on MG. Experimental findings for the traditional control method and suggested control approach corroborate the theoretical analysis. It has been shown that the advised control method is effective. Finally, a seamless switch to island mode is made possible. We have decreased harmonics from 8% to 3% (less than 5%) during the amplification process in accordance with IEEE standards. Thus, by lowering harmonics, unpredictable behaviour is decreased and seamless transition is made possible.

6. REFERENCES

[1] J. Rocabert, A. Luna, F. Blaabjerg, and P. Rodríguez, "Control of power converters in AC microgrids," *IEEE Trans. Power Electron.*, vol. 27, no. 11, pp. 4734–4749, Nov. 2012.

[2] T. L. Vandoorn, J. C. Vasquez, J. De Kooning, J. M. Guerrero, and L. Vandeveld, "Microgrids: Hierarchical control and an overview of the control and reserve management strategies," *IEEE Ind. Electron. Mag.*, vol. 7, no. 4, pp. 42–55, Dec. 2013.

[3] A. H. Etemadi and R. Iravani, "Supplementary mechanisms for smooth transition between control modes in a microgrid," *Elect. Power Syst. Res.*, vol. 142, pp. 249–257, Jan. 2017.

[4] S. Sajadian and R. Ahmadi, "Model predictive control of dual-mode operations z-source inverter: Islanded and grid-connected," *IEEE Trans. Power Electron.*, vol. 33, no. 5, pp. 4488–4497, May 2018.

[5] S. M. Ashabani and Y. A.-R. I. Mohamed, "A flexible control strategy for grid-connected and islanded microgrids with enhanced stability using nonlinear microgrid stabilizer," *IEEE Trans. Smart Grid*, vol. 3, no. 3, pp. 1291–1301, Sep. 2012.

[6] J. Kim, J. M. Guerrero, P. Rodriguez, R. Teodorescu, and K. Nam, "Mode adaptive droop control with virtual output impedances for an inverter-based flexible AC microgrid," *IEEE Trans. Power Electron.*, vol. 26, no. 3, pp. 689–701, Mar. 2011.

[7] J. Wang, N. C. P. Chang, X. Feng, and A. Monti, "Design of a generalized control algorithm for parallel inverters for smooth microgrid transition operation," *IEEE Trans. Ind. Electron.*, vol. 62, no. 8, pp. 4900–4914, Aug. 2015.

[8] Y. A.-R. I. Mohamed and A. A. Radwan, "Hierarchical control system for robust microgrid operation and seamless mode transfer in active distribution systems," *IEEE Trans. Smart Grid*, vol. 2, no. 2, pp. 352–362, Jun. 2011.

[9] X. Li, H. Zhang, M. B. Shadmand, and R. Balog, "Model predictive control of voltage source inverter with seamless transition between islanded and grid-connected operations," *IEEE Trans. Ind. Electron.*, vol. 64, no. 10, pp. 7906–7918, Oct. 2017.

[10] H. Mahmood and J. Jiang, "A control strategy of a distributed generation unit for seamless transfer between grid connected and islanded modes," in *Proc. Ind. Electron. (ISIE)*, 2014, pp. 2518–2523.

AUTHOR'S PROFILE



Ms. Tatheer Banu received her B.Tech from Vasireddy Venkatadri Institute of Technology, Guntur in 2020. Presently she is pursuing M.Tech in Vidya Jyothi Institute of Technology, Hyderabad. Her areas of interest are Power Systems, Power Quality.

Email Id- tatheerasbt@gmail.com.



Dr. A. Srujana completed her Bachelor's degree from Kakatiya Institute of Technology & Science, Warangal, and M. Tech in Power Electronics from JNTU, Hyderabad. She has worked at various capacities in prominent Engineering colleges as Principal, Professor and HOD. She has guided fifteen M. Tech projects & is guiding four Ph. D students. Her expertise in research is witnessed with her publication of 24 research papers in core technical areas in indexed journals and also in both National and International peer reviewed conferences. She has about 24 years of experience in Academics. Her areas of interests are power Electronics, FACTS, HVDC and POWER SYSTEMS.

Email Id- eeehod@vjit.ac.in